Electronic Supplementary Material (ESI) for Journal of Materials Chemistry A.

# Supporting Information

## Facilitating Redox Reaction of Polysulfides by An Electrocatalytic Layer-modified Separator for Lithium Sulfur Batteries

Pengjian Zuo,[a]* Junfu Hua,[a] Mengxue He,[a] Han Zhang,[a] Zhengyi Qian,[a] Yulin Ma,[a] Chunyu Du,[a] Xinqun Cheng,[a] Yunzhi Gao,[a] Geping Yin[a]

[a]Institute of Advanced Chemical Power Source, School of Chemistry and Chemical Engineering, Harbin Institute of Technology, Harbin 150001, China

*E-mail: zuopj@hit.edu.cn

# 1. Experiment section

## 1.1 Visualized adsorption of polysulfides

$Li_2S_6$ in nominal stoichiometry, a representative of polysulfides, was synthesized by mixing sulfur and lithium sulfides ($Li_2S$) at a molar ratio of 5:1 in a solvent of DOL:DME (1:1 in a volume ratio) followed by vigorous magnetic stirring for 24 h at 50 ℃. The concentration of $Li_2S_6$ was 0.33 M. 20 μL $Li_2S_6$ solution added into 4 mL DOL/DME solvent as standard solution. KB, activated KB, KB@Ir-10 and KB@Ir-30 with the same surface area of 12 $m^2$ were added to the standard solutions. The resting time for the sediment of the adsorbents was 1 h after stirring.

## 1.2 Preparation of KB@Cu composite

Copper dinitrate was first dissolved in ethanol alcohol to form a 20 wt% $Cu(NO_3)_2$ content solution ($Cu(NO_3)_2$/EtOH-solution). An ultrasonic-assisted multiple wetness impregnation and rotary evaporation method was applied to mix copper dinitrate and activated KB, i.e. the copper dinitrate solution was first dropped into the activated KB and subsequently sonicated for 1 h, ensuring that the $Cu(NO_3)_2$ is uniformly infiltrated in KB. Then the solution was heated through oil bath at 60 °C to evaporate the solvent. This process was repeated until a certain amount of $Cu(NO_3)_2$ was added to KB. The resulting sample was then reduced at 600 °C for 6 h with a heating rate of 5 °C $min^{-1}$ under argon mixed with 5% hydrogen environment.The 30 wt% Cu in KB@Cu was designed.

## 1.3 Preparation of sulfur cathode

KB/S composites were prepared as cathode. Sulfur powder (Aladdin) was first dissolved in carbon disulfide ($CS_2$) to form a 10 wt% solution. KB was added into sulfur-$CS_2$ solution, followed by sonication for 10 min to form homogeneous slurry. Then the slurry was stirred under ambient temperature to evaporate $CS_2$. The obtained powder (80 wt% sulfur) was ground and heated at 155 °C for 12 h in in flowing argon. Final sulfur content was determined by the thermogravimetric analysis (TGA). The sulfur cathodes were prepared by shaker-milling of KB/S (80 wt%), Super P (10 wt%) and PVDF (10 wt%) in NMP. The well-mixed slurries were coated onto an aluminum foil current collector by doctor blading. The obtained cathodes were punched into circular disks of 12 mm after drying in an oven at 50 °C for 24 h. The areal sulfur loading of the sulfur cathodes used for the main electrochemical tests was around 0.8 mg $cm^{-2}$. For the evaluation of the areal capacity, a cathode used water-soluble binder with PEO : PVP : GA (Arabic gum) ratio of 4 : 1 : 1 wt%. The KB/S : Super P : binder was 7 : 2 : 1 and an areal sulfur loading of 4.62 mg $cm^{-2}$ was used.

## 1.4 Symmetrical cell assembly and measurements

The electrodes for symmetrical cells were fabricated without the presence of elemental sulfur. Each host material (KB and KB@Ir) and PVDF binder at a weight ratio of 3:1 were dispersed in NMP. Slurry was produced under stirring and was coated on aluminum foils. Electrode disks with a diameter of 14 mm were punched out of slurry-coated aluminum foils after thorough drying. Those disks were used as identical working and counter electrodes, while 20 μL electrolyte containing 0.33 M $Li_2S_6$ and 1 M LiTFSI dissolved in DOL/DME (v/v = 1/1) was added. CV measurements of the symmetrical cells were performed at scan rate of 20 mV $s^{-1}$ from -0.8 V to 0.8 V. Electrochemical impedance spectroscopy (EIS) tests were conducted on PARSTAT 2273 electrochemical workstation with frequency range of 10 kHz - 10 mHz. The Tafel tests were carried out using CHI 604D workstation from -0.25 V to 0.25 V with at scan rate of 0.1 mV $s^{-1}$. The Cyclic voltammetry curves of the liquid Li-S batteries were recorded with lithium foil as the anode and each host material (KB and KB@Ir) as cathod at a scanning rate of 0.1 mV·$s^{-1}$ at 1.5-3.0 V using AUTOLAB PGSTAT302N instrument. The electrolyte was 0.33 M $Li_2S_6$ and 1 M LiTFSI dissolved in DOL/DME (v/v = 1/1).

## 1.5 Calculations

All density functional calculations were performed using the Guassian09 program package [1]. No geometric constraints were assumed in geometry optimization. All structures were optimized and characterized at B3LYP/LANL2DZ. The nonlocal correlation functional of Lee, Yang, and Parr [2] (B3LYP) with the 6-31++G** basis set was used for S atom [3], and the Los Alamos effective core pseudo-potentials (ECP) basis set LANL2DZ was used for the Ir, Li atoms. All reported charges are Mulliken local charges (Au). The relative energies of the reactants and adsorption states presented in this study were zero-point-energy (ZPE) obtained from frequency calculations at the same level of optimization. All stationary points were characterized as the minima (no imaginary frequency) via Hessian calculation. The adsorption energies ($E_{ads}$) for polysulfide adsorbed on isolated $Ir_4$ cluster were calculated as the following definitions.

$$E_{ads} = E_{system} - E_{Ir4} - E_{Li2Sx}$$

$E_{system}$ is the total energy of adsorption system; $E_{Ir4}$ and $E_{Li2Sx}$ denote the energy of $Ir_4$ and $Li_2S_x$ respectively.

## 2. Supplementary Figures and Discussion

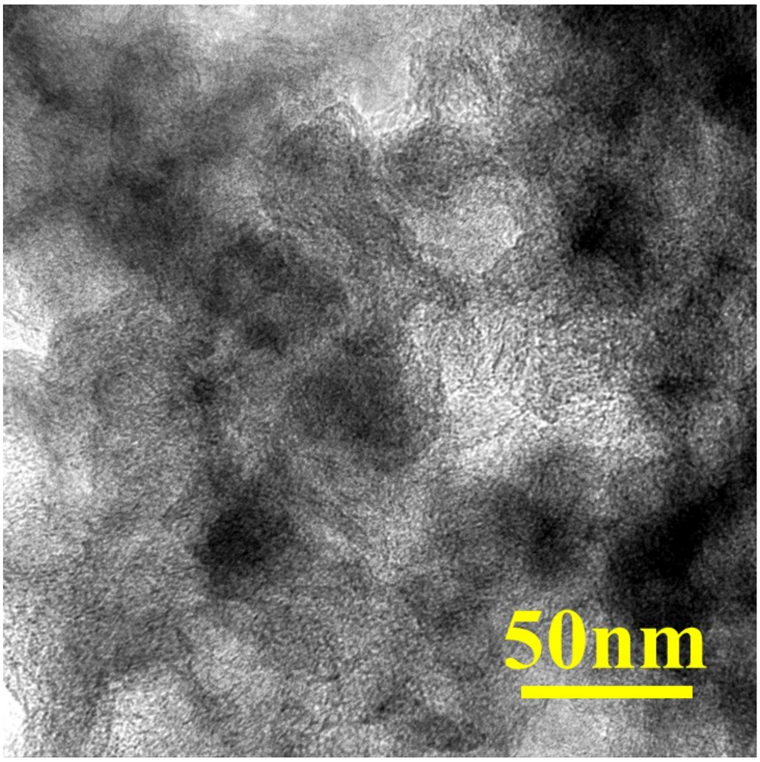

Fig.S1 TEM image of activated KB.

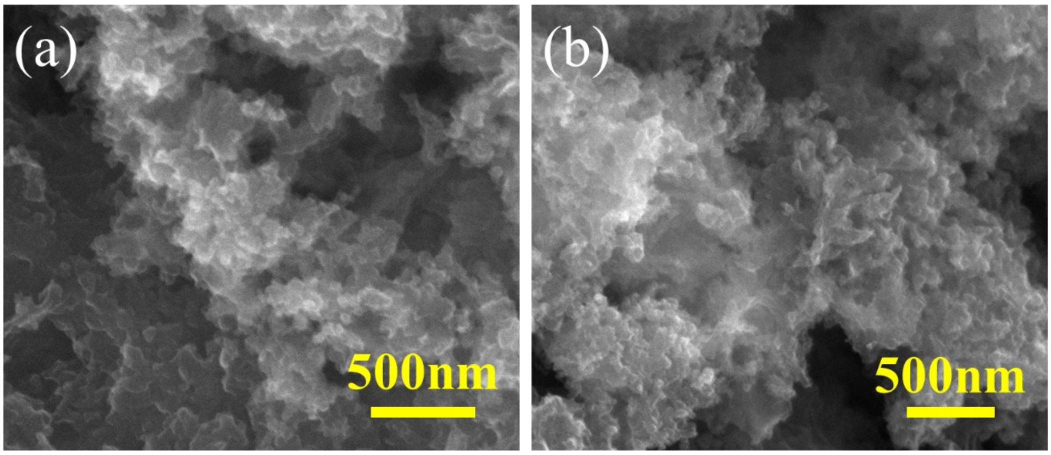

Fig. S2 SEM images of (a) KB@Ir-10 and (b) KB@Ir-30.

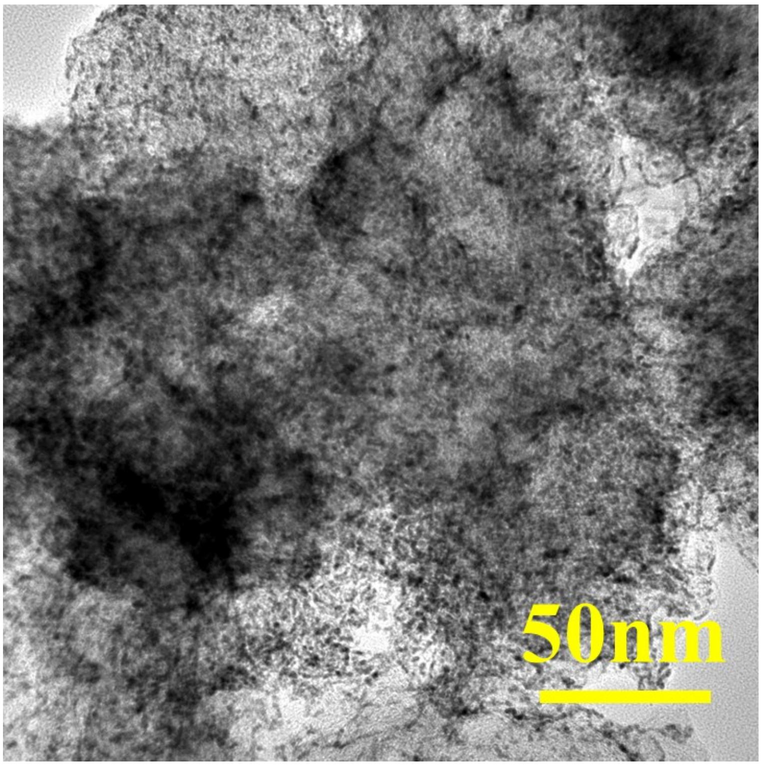

Fig. S3 TEM image of KB@Ir-30.

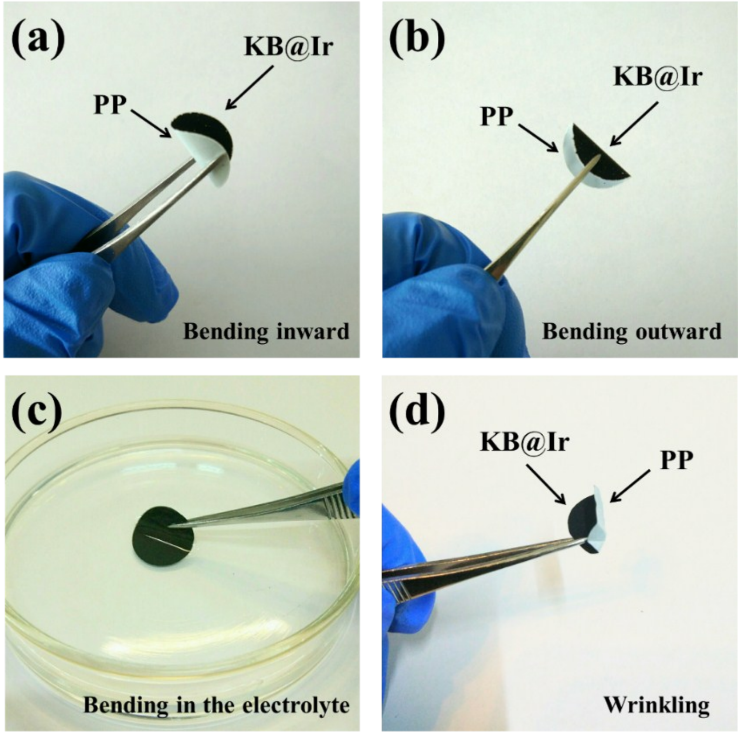

Fig. S4 Digital pictures of KB@Ir separator under various mechanical stress: (a) bending inward; (b) bending outward; (c) bending in the electrolyte; (d) wrinkling..

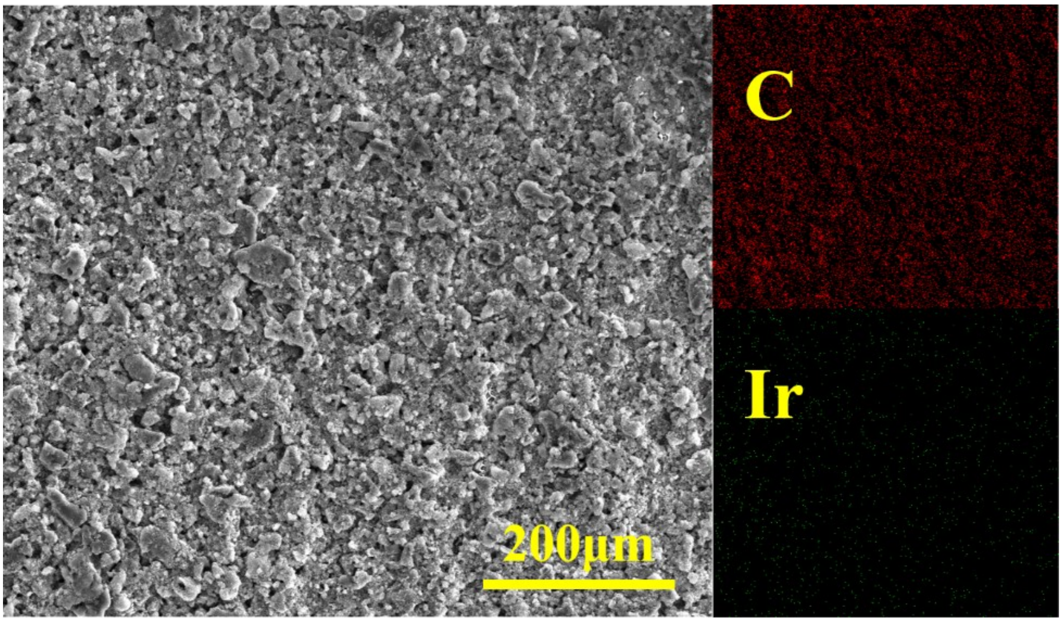

Fig. S5 The energy dispersive spectroscopic (EDS) mapping images of KB@Ir separator surface for C and Ir.

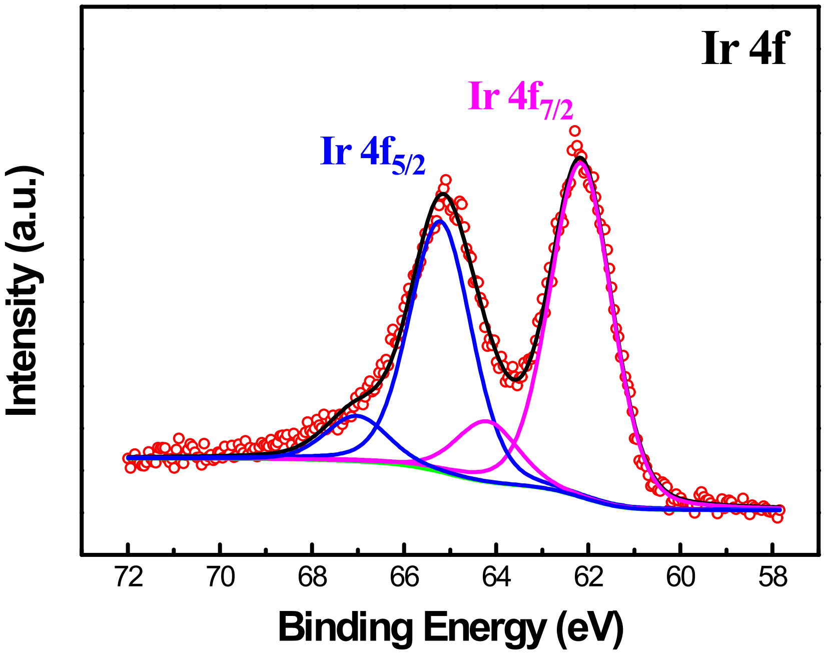

Fig. S6 The Ir 4f XPS survey spectra of KB@Ir composites.

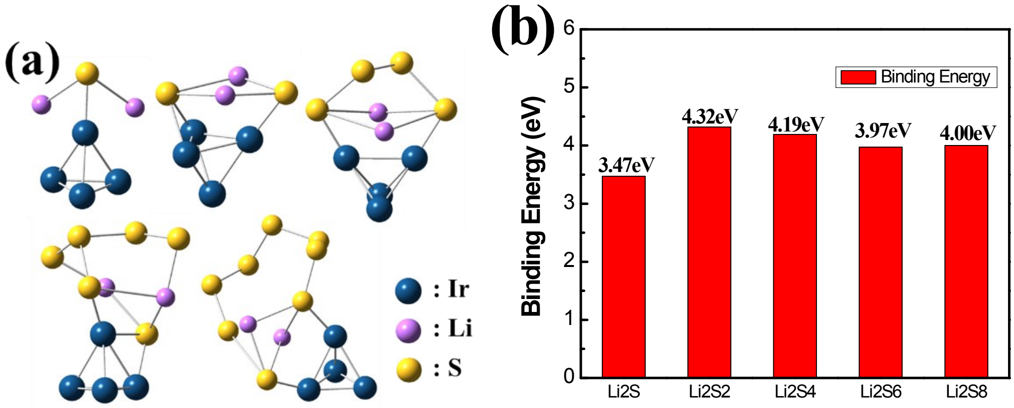

Fig. S7 (a) Binding geometries and (b) binding energies of a polysulfides molecule on iridium cluster, which is derived from theoretical calculation based on DFT.

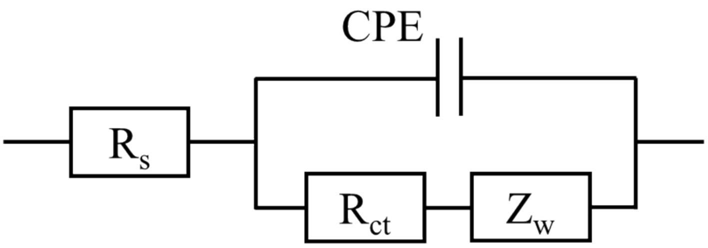

Fig. S8 Equivalent circuit used for fitting the EIS spectra of symmetrical cells.

Table S1 The fitting results of EIS spectra of symmetrical cells.

| **Materials** | **$R_s$ (ohm)** | **$R_{ct}$ (ohm)** |
|---|---|---|
| KB | 2.191 | Around 3800 |
| KB@Ir-10 | 2.199 | 216.9 |
| KB@Ir-30 | 2.569 | 181.6 |

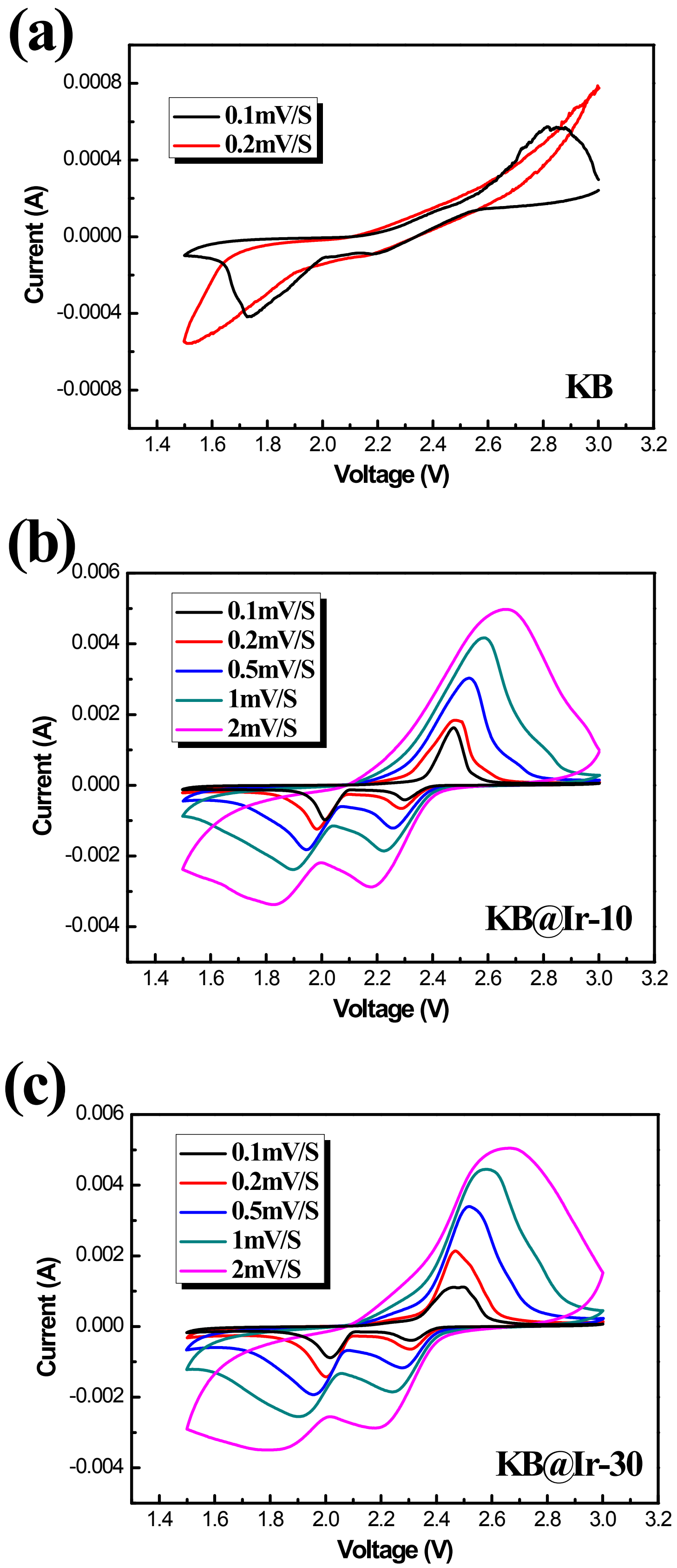

Fig. S9 CV curves of (a) KB, (b) KB@Ir-10 and (c) KB@Ir-30 cathodes at different sweep rates.

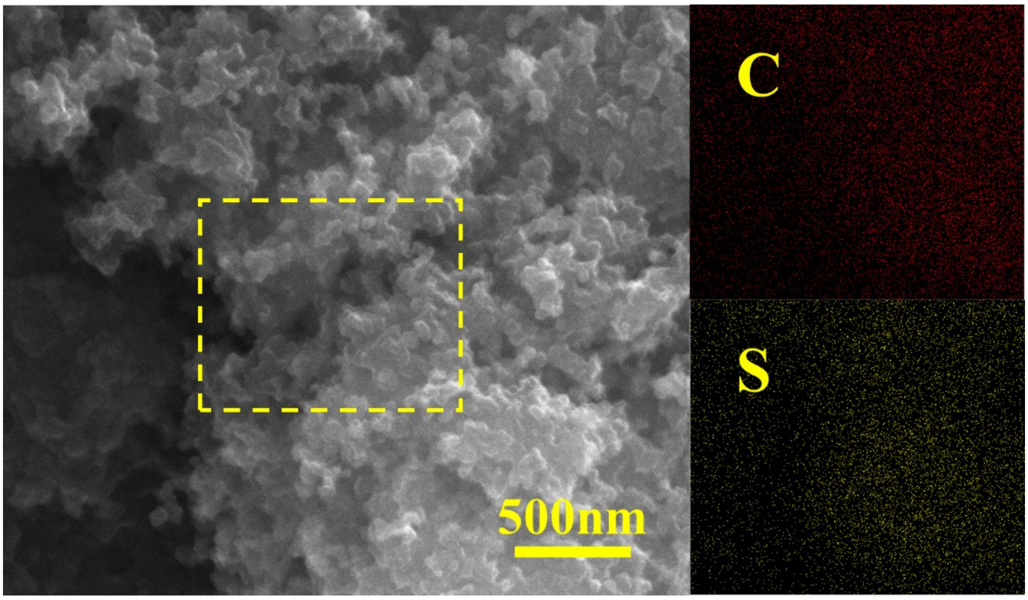

Fig. S10 The energy dispersive spectroscopic (EDS) mapping images of KB/S cathode for C and S.

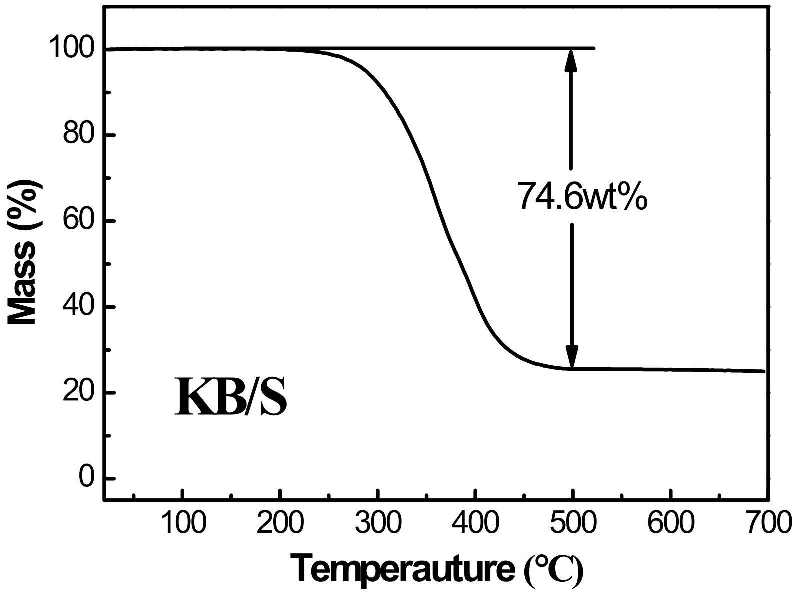

Fig. S11 TGA curves of KB/S composite under argon atmosphere.

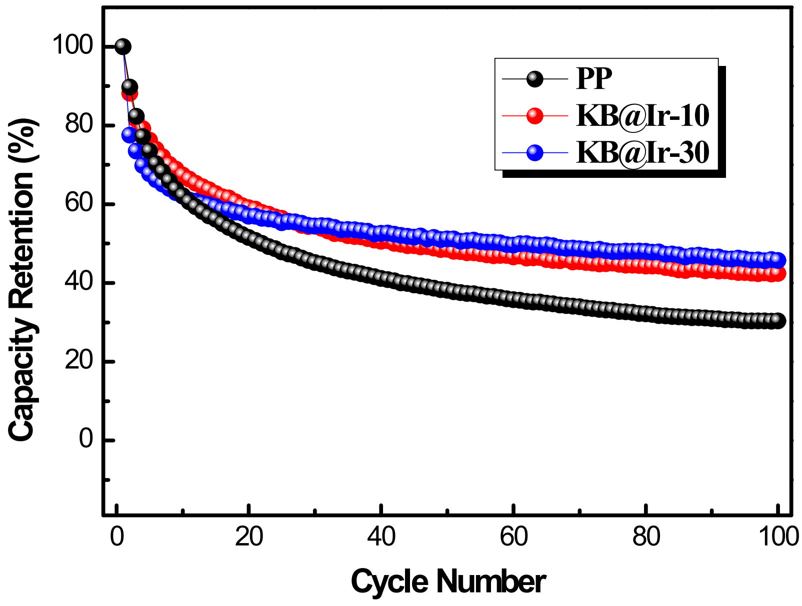

Fig. S12 Stability of composite cathodes. Capacity retention of KB/S cathodes with separators of PP, KB@Ir-10, and KB@Ir-30.

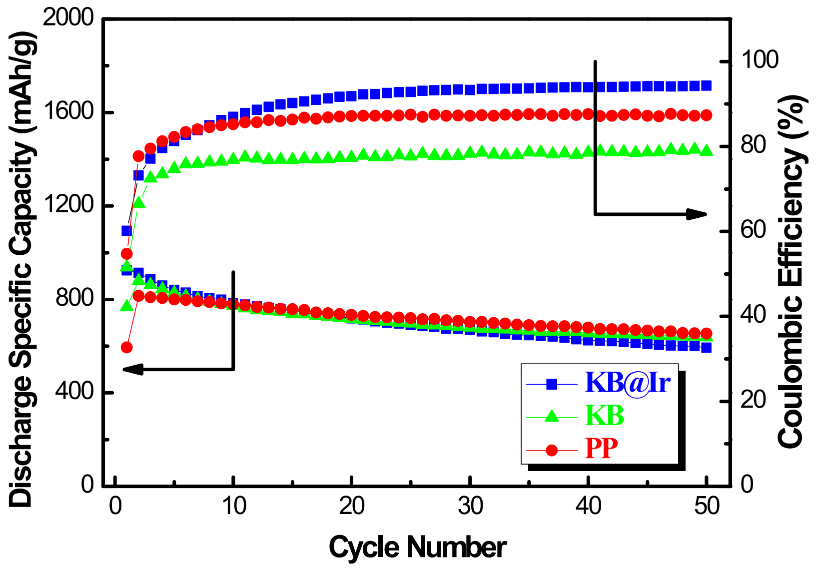

Fig. S13 Electrochemical performance of KB/S cathodes with different separators, while the electrolyte contained no $LiNO_3$.

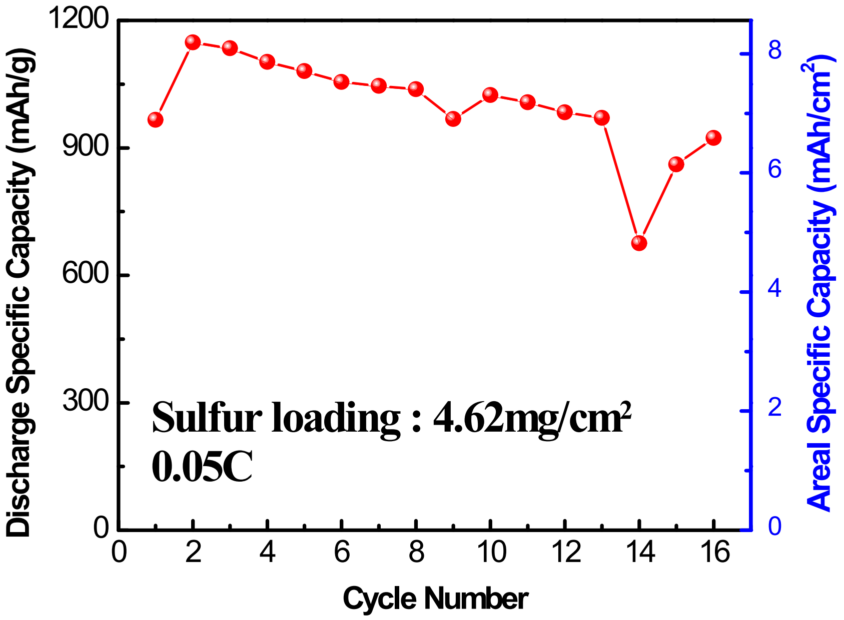

Fig. S14 Performance of high-sulfur-loading electrodes with KB@Ir-30 catalyst layer at 0.05 C.

## KB@Ir as separator coating or host material of sulfur cathode

We have tested the electrochemical performance of sulfur cathode with the KB@Ir as host material. The Figure S15 is the XRD patterns of the KB@Ir/S, KB/S, KB and S. Compared with the diffraction peaks of elemental sulfur, the perfectly matched diffraction peaks could be detected from the KB@Ir/S and KB/S composites, indicating that the iridium nanoparticles did not react with the elemental sulfur in the process of heat treatment. Figure S16 is the electrochemical performance with KB@Ir as separator coating and host material, respectively. It can be clearly seen that, compared with the KB/S composites, the better cycle performances are achieved for the lithium sulfur battery with KB@Ir as separator coating and host material. Furthermore, the cells with KB@Ir as separator coating deliver the highest specific capacity at 0.2 C and 1 C. The excellent electrochemical performance of the lithium sulfur battery with KB@Ir as separator coating results from the strong interaction of iridium nanoparticles with polysulfides and the improved redox kinetics of polysulfides during charge/discharge process. The room between the sulfur cathode and KB@Ir coating can be acted a reservoir for lithium polysulfides, which is beneficial to facilitate sufficient contact of iridium nanoparticle catalysts with polysulfides and improve the redox kinetics of polysulfides during charge/discharge process, resulting in the excellent electrochemical performance of the lithium sulfur battery with KB@Ir as separator coating.

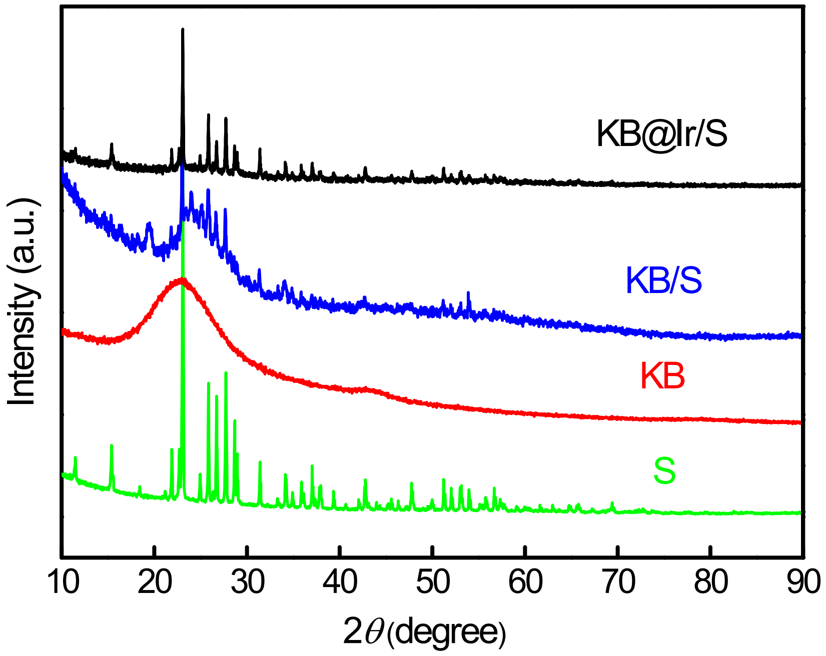

Fig. S15. The XRD patterns of the samples.

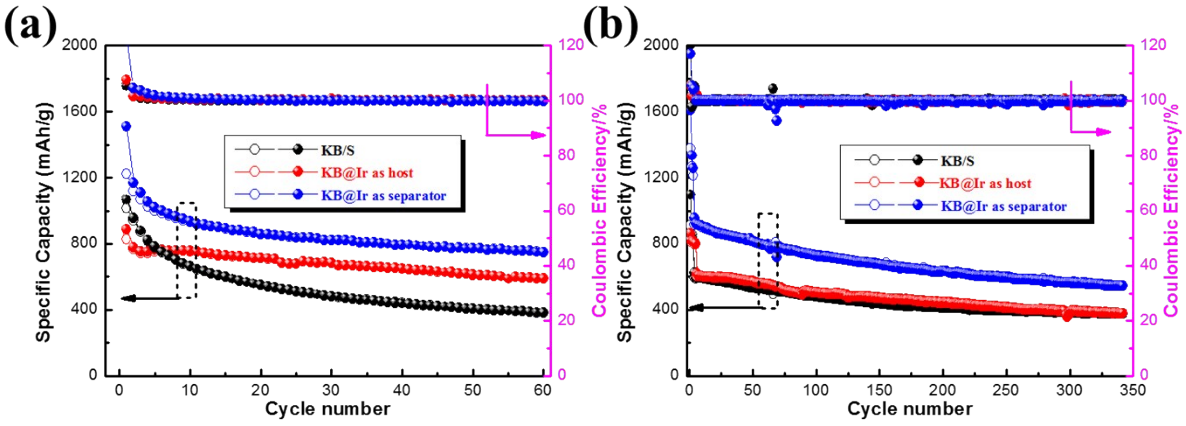

Fig. S16. The electrochemical performance with KB@Ir as separator coating and host material. Cycle performance at (a) 0.2 C and (b) 1 C.

## KB@Cu and KB@Ir as separator coating

In order to further compare the effect of Ir and other metal particles (such as the low-cost Cu) especially in the cathode material (sulfur content > 70 wt%) with mesoporous structure and conventional ether-based electrolyte for lithium sulfur batteries, we have prepared the KB@Cu composites (~30 wt% for comparison ) using ultrasonic-assisted multiple wetness impregnation and rotary evaporation technique. The strong interaction between Cu metal and sulfur species has been confirmed by Wang's group to be effective for improving the sulfur content (from 30 to 50 wt%) and charge/discharge efficiency, especially for the microporous-structured cathode composite in the conventional carbonate electrolyte[4]. The XRD pattern of the composite is shown in Figure S17. The XRD results confirm that the Cu is deposited into mesoporous KB matrix. Figure S18 is the visualized adsorption of KB/Cu and KB/Ir composites with the same surface area in the sealed vials containing $Li_2S_6$ solution for 1 h. It should be noticed that the color of the solution containing KB@Cu shows slight discoloration compared with the pristine $Li_2S_6$ solution, confirming the relatively weak interaction between the Cu nanoparticles and $Li_2S_6$. Figure S19 shows the cycle performance of the lithium sulfur battery with the separator modified by KB@Cu and KB@Ir respectively. Compared with the cell with KB@Ir-modified separator, the cell with KB@Cu as separator coating performs relatively lower specific capacity and rate performance, which is mainly related to the stronger interaction of Ir with polysulfides and the improved redox kinetic of polysulfides by the catalysis of Ir during cycling. In consideration of cost, the Ir-based alloy/composite nanoparticle may be promising in the high performance sulfur cathode for lithium sulfur batteries.

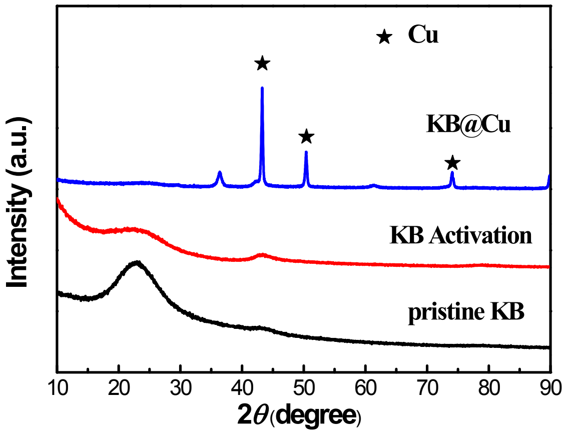

Fig. S17. The XRD pattern of KB@Cu.

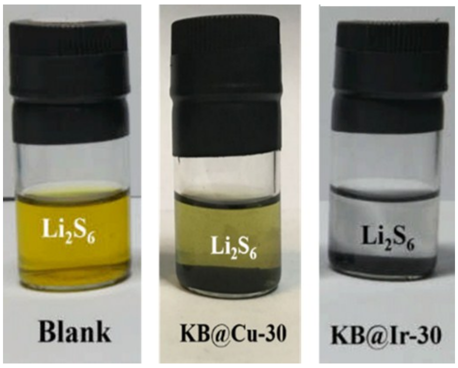

Fig. S18. Visualized adsorption of of KB/Cu and KB/Ir composites with the same surface area in the sealed vials containing Li2S6 solution for 1 h.

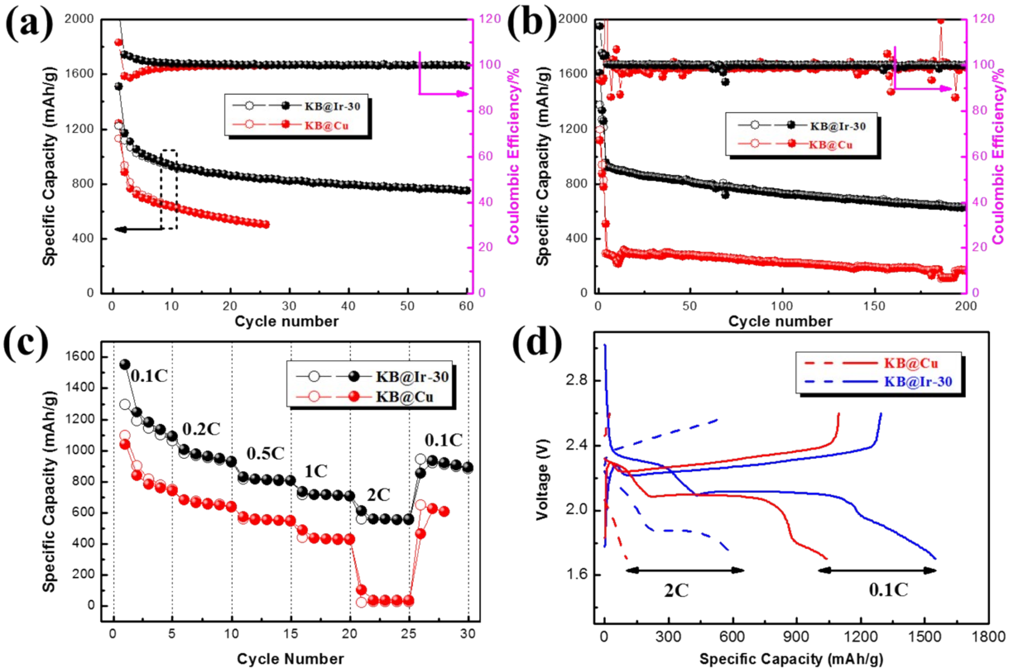

Fig. S19. The electrochemical performance with KB@Cu as separator coating compared with KB@Ir as separator coating.

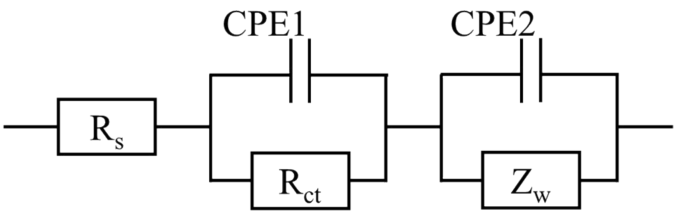

Fig. S20 Equivalent circuit used for fitting the EIS spectra of fresh cells.

Table S2 The fitting results of EIS spectra of fresh cells.

| **Materials** | **$R_s$ (ohm)** | **$R_{ct}$ (ohm)** |
|---|---|---|
| KB/S | 1.628 | 273.40 |
| KB | 5.904 | 127.6 |
| KB@Ir-10 | 4.095 | 50.86 |
| KB@Ir-30 | 6.780 | 34.26 |

## 4. Supplementary References:

1 M. J. Frisch, G. W. Trucks, H. B. Schlegel, G. E. Scuseria, M. A. Robb, J. R. Cheeseman, G. Scalmani, V. Barone, B. Mennucci, G. A. Petersson, H. Nakatsuji, M. Caricato, X. Li, H. P. Hratchian, A. F. Izmaylov, J. Bloino, G. Zheng, J. L. Sonnenberg, M. Hada, M. Ehara, K. Toyota, R. Fukuda, J. Hasegawa, M. Ishida, T. Nakajima, Y. Honda, O. Kitao, H. Nakai, T. Vreven, J. A. Montgomery Jr., J. E. Peralta, F. Ogliaro, M. Bearpark, J. J. Heyd, E. Brothers, K. N. Kudin, V. N. Staroverov, R. Kobayashi, J. Normand, K. Raghavachari, A. Rendell, J. C. Burant, S. S. Iyengar, J. Tomasi, M. Cossi, N. Rega, J. M. Millam, M. Klene, J. E. Knox, J. B. Cross, V. Bakken, C. Adamo, J. Jaramillo, R. Gomperts, R. E. Stratmann, O. Yazyev, A. J. Austin, R. Cammi, C. Pomelli, J. W. Ochterski, R. L. Martin, K. Morokuma, V. G. Zakrzewski, G. A. Voth, P. Salvador, J. J. Dannenberg, S. Dapprich, A. D. Daniels, Ö. Farkas, J. B. Foresman, J. V. Ortiz, J. Cioslowski and D. J. Fox, Gaussian 09, Gaussian, Inc., Wallingford CT, 2010.

2 C. Lee, W. Yang and R. G. Parr, *Phys. Rev. B*, 1988, **37**, 785-789.

3 M. Andersson and P. Uvdal, *J. Phys. Chem. A*, 2005, **109**, 2937–2941.

4 S. Zheng, F. Yi, Z. Li, Y. Zhu, Y. Xu, C. Luo, J. Yang and C. Wang, Adv. Func. Mater., 2014, 24, 4156-4163.